文章编号：1001-9014(2022)01-0139-12

DOI:10.11972/j.issn.1001-9014.2022.01.010

Progress on nBn infrared detectors

SHI Qian[1,2,3], ZHANG Shu-Kui[2,3*], WANG Jian-Lu[2,3,4,5*], CHU Jun-Hao[3,4]

(1. Shanghai Institute Optics and Fine Mechanics, Chinese Academy of Sciences, Shanghai 201800, China;
2. Hangzhou Institute for Advanced Study, University of Chinese Academy of Sciences, Hangzhou 310024, China;
3. State Key Laboratory of Infrared Physics, Shanghai Institute of Technical Physics, Chinese Academy of Sciences, Shanghai 200083, China;
4. Institute of Optoelectronics, Shanghai Frontier Base of Intelligent Optoelectronics and Perception, Fudan University, Shanghai 200433, China;
5. Frontier Institute of Chip and System, Fudan University, Shanghai 200433, China)

Abstract: The nBn infrared (IR) detector is designed to eliminate the Shockley-Read-Hall (SRH) generation-recombination (G-R) currents, which will effectively reduce the dark current and increase the operating temperature of the detector. Due to the compatibility of the manufacturing process and the existence of a substrate with a perfectly matched lattice, the nBn infrared detectors based on III－V compounds including type－II superlattice (T2SLs) materials have been developed rapidly. Through theoretical simulation, the nBn infrared detector based on the HgCdTe material system can also effectively suppress the dark current. However, the difficulty of removing the valence band barrier hinders HgCdTe nBn infrared detector development. This review will elaborate on the physical mechanism of nBn detectors to suppress dark current, and then introduce the development status and development trend of nBn barrier detectors in different semiconductor materials.

Key words: nBn infrared detector, Sb-based III-V semiconductor, type-II superlattice, HgCdTe

nBn红外探测器研究进展

石 倩[1,2,3], 张书魁[2,3*], 王建禄[2,3,4,5*], 褚君浩[3,4]

(1. 中国科学院上海光学精密机械研究所,上海 201800;
2. 中国科学院大学杭州高等研究院 物理与光电工程学院,浙江 杭州 310024;
3. 中国科学院上海技术物理研究所 红外物理国家重点实验室,上海 200083;
4. 复旦大学 光电研究院 上海市智能光电与感知前沿科学研究基地,上海 200433;
5. 复旦大学 芯片与系统前沿技术研究院 上海 200433)

摘要:nBn红外探测器旨在消除肖特基-里德-霍尔产生复合电流,这将有效降低器件的暗电流并提高工作温度。由于制造工艺的兼容性和晶格匹配的衬底的存在,基于III-V化合物(包括二类超晶格材料)的nBn红外探测器得到了快速发展。通过理论模拟,基于HgCdTe材料的nBn红外探测器也能有效抑制暗电流。然而,去除价带势垒的困难阻碍了HgCdTe nBn器件的发展。本综述将阐述nBn探测器抑制暗电流的物理机制,并介绍nBn探测器在不同材料体系中的发展现状和趋势。

关 键 词:nBn红外探测器;Sb基III-V族半导体;二类超晶格;碲镉汞

中图分类号:TN2　　**文献标识码**:A

Received date: 2021-12-26, **revised date**: 2022-01-10　　**收稿日期**:2021-12-26,**修回日期**:2022-01-10

Foundation items: Supported by the National key research and development program during the "14th Five-Year Plan" (2021YFA1200700), Natural Science Foundation of China (62025405 and 61835012), Strategic Priority Research Program of the Chinese Academy of Sciences (XDB44000000), Science and Technology Commission of Shanghai Municipality (2151103500).

Biography: SHI Qian (1994-), female, master. Research area involves high temperature infrared detectors. E-mail: shiqian20@mails.ucas.ac.cn

* **Corresponding authors**: E-mail: zhangshukui@ucas.ac.cn, jianluwang@fudan.edu.cn

Introduction

Infrared detectors are widely applied in communications, medical treatment, astronomical observation, infrared imaging, night vision, and guidance[1-3]. With the development of society, the demands for infrared detectors have become diversified, which has continuously promoted the development of infrared detection technology. Infrared detectors have developed from the first generation to the third generation, and the detection mechanism is constantly improving and developing (as shown in Fig. 1). At present, the new generation of infrared detection technology is developing in the direction of large area array, two-color and multi-color, digitization, high frame rate, hyperspectral and single-photon detection[4]. The core competitiveness will focus on the concept of "SWaP": smaller size, lower weight, and lower power consumption[5-7].

In order to suppress the influence of dark current, the infrared detector needs to work at or below the liquid nitrogen temperature, which greatly increases the weight and power consumption of the detectors and reduces the reliability[8]. Therefore, increasing the operating temperature of infrared detectors is an important research direction. If the temperature required for normal operation of the detector is increased, not only can the purpose of "SWaP" be achieved, but also the startup speed of the device can be accelerated. It can also significantly increase the reliability of the detector. Considerable efforts have been made aiming to increase detector operating temperatures to realize high-operating temperature (HOT) detectors over the past decades[9]. Among the new emerging strategies cascade infrared detectors[10, 11], InAs/GaSb type-II superlattices (T2SLs)[12], and barrier structures[13] have considerable progress.

In 2006, Maimon and Wicks proposed the nBn structure device for the first time, and developed it on a short-wave infrared detector, using InAs material as the absorbing layer and AlAsSb as the barrier layer[14]. Subsequently, the nBn structure was applied to InSb[15-17], InAsSb[18-21], T2SLs[22-29], and HgCdTe[30-35] detectors. Related technologies have been developed, and some products have been applied. The nBn detector is designed to block the flow of majority carriers through reasonable energy band structural design, while minority carriers can flow freely. Fig. 2(a) shows the schematic diagram of the energy band structure of nBn detector. It consists of an absorbing n-type layer, a large bandgap barrier layer, and a thin n-type contact layer. The thickness of the absorbing layer should be comparable to the absorption length of light in the device which is typically several microns, while the contact layer is for biasing the device. There is a special type of heterojunction between the barrier layer and the n-type layers: all the bandgap difference appears in the conduction band offset which blocks the flow of majority carrier electrons, and there is zero valence band offset which allows the free passage minority carrier holes[23]. To suppress the dark current effectively, the barrier should be located near the minority carrier collector and away from the region of optical absorption[36]. Placing the barrier in this location allows photogenerated holes to flow unimpeded to the contact while majority carrier dark currents, re-injected photo-current, and surface currents are all blocked. Besides, the same doping type in the barrier and active layers is the key to maintaining a low, diffusion-limited dark current[37].

Dark current is an important indicator that restricts the detection performance of IR detectors. Generally, the composition of dark current is very complex, which includes diffusion current, G-R current, tunneling current that includes direct tunneling current and trap-assisted tunneling current, etc. In addition, due to surface defects and non-ideal electrodes of the device, there are surface leakage currents[38, 39]. The magnitude of the G-R current is linearly related to the intrinsic carrier concentration, while the diffusion current is proportional to the square of the intrinsic carrier. As the operating temperature rises, the intrinsic carrier concentration of the mate-

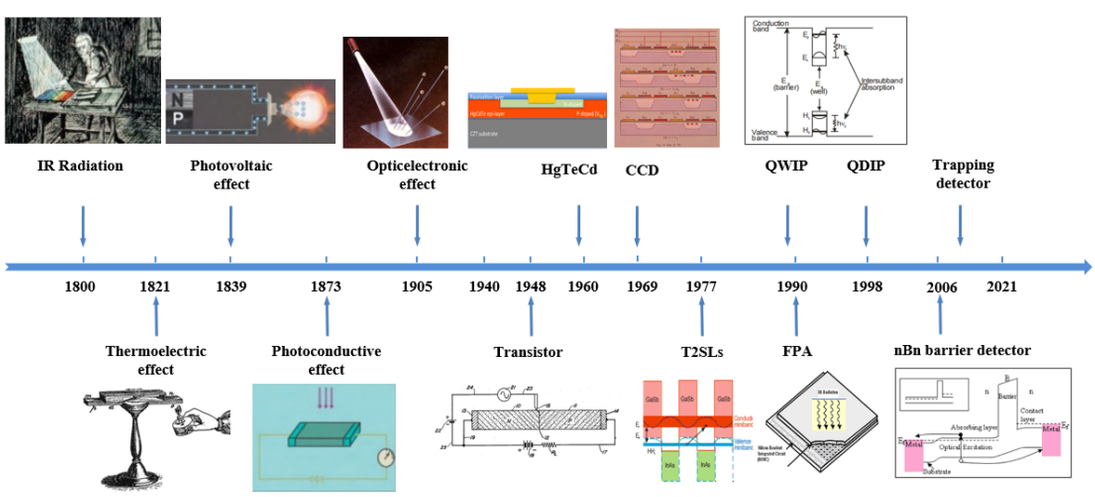

Fig. 1 History of the development of infrared detectors
图1 红外探测器的发展史

rial will also increase significantly, and the dark current of the device will transfer from the recombination limit to the diffusion limit.

Generally, the G-R current is derived from the thermal excitation and recombination of carriers that occur in the depletion region of the p-n junction. And the SRH current is the G-R current which caused by the defect centers in the depletion region. Impurities and defects in semiconductors will form certain energy levels in the forbidden band which can promote the excitation and recombination of carriers. The nBn detectors with a large bandgap barrier layer will increase the energy required for electrons to transition to the impurity and defect levels, thereby suppressing the generation of SRH current. Due to the restriction of the growth process, surface passivation process, sample shape, and other external factors, surface leakage will also be introduced, and it may even become the dominant mechanism of device dark current. The surface leakage current in nBn detectors is suppressed by its multi-carrier barrier[40, 41]. The spatial makeups of current components in nBn detectors are shown in Fig 2(b). The diffusion current is formed by the diffusion and drift of carriers on both sides of the depletion region of the p-n junction under the action of an electric field. Auger recombination[42] is that when a carrier transitions from a high energy level to a low energy level or recombines through a bandgap, the released energy is transferred to another carrier and transitions to a higher energy level. Owing to Auger diffusion currents being generated in the same region as the photocurrents in nBn barrier detector, Auger currents share the same spatial makeup as the photocurrent[43]. Fig. 2(c) is the current components of traditional p-n photodiode. The majority-carrier dark current, surface leakage currents, and SRH generation current can almost be eliminated because of the existence of the unipolar barrier layer.

The typical Arrhenius plot of the dark currents as a function of temperature in nBn detector and in a conventional diode is shown in Fig. 2(d). Generally, the diffusion current varies as $T^{3}\exp(-E_{g0}/kT)$, while the G−R current varies as $T^{3/2}\exp(-E_{g0}/2kT)$ which is dominant by the generation of electrons and holes by SRH traps in the depletion region. (E_{g0} is the bandgap extrapolated to zero temperature, T is the temperature, and k is Boltzmann's constant). T_c is defined as the crossover temperature at which the diffusion and G-R currents are equal[44]. Consequently, the dark current is then limited to the diffusion contribution. The slope of the lower portion of the Arrhenius plot for the standard photodiode is roughly half that of the upper portion. The properties of the nBn detector (blue line) show the extension of the high-temperature diffusion-limited region to temperatures below T_c. In the low-temperature region, nBn detector has a lower dark current than the conventional photodiode. Compared to the conventional photodiode, it should exhibit a higher signal-to-noise ratio at the same temperature and operate at a higher temperature with the same dark current. Moreover, the Teledyne Technologies published an empirical expression in 2007, called "Rule 07", for estimation the performance of state-of-the-art HgCdTe photodiodes dark current versus normalized wavelength-temperature product ($\lambda_c T$)[45]. Hereafter, Lee et al. suggested replacing Rule 07 by Law 19 corresponding exactly to the background limited curve for room temperature[46]. The internal photodiode current may be several orders orf magnitude below Rule 07 versus given cut-off wavelength and operating temperature. Ideal nBn barrier detectors are expected to exhibit diffusion limited performance originating from Auger 1 generation matching Rule 07[47]. To date, however, experimentally prepared barrier devices still show diffusion limited performance.

Compared to the conventional p-n photodiode, because of the near elimination of SRH and surface leakage currents, the nBn photodetector requires less cooling to operate optimally and has simpler processing requirements. Under the conditions of lattice matching and energy band matching, the nBn structure could be extended to different material systems which will be discussed in later chapters.

1 Research status

1.1 III – V compounds barrier detectors

III-V materials can provide stronger chemical bonds, and the band edge is less dependent on the composition, hence it has higher chemical stability[48]. Furthermore, considering the cost of detector materials, III-V materials have great advantages. The diameter of the antimonide material wafer reaches the order of 10 cm, so the detectors fabricated by III-V compounds with larger areas and higher uniformity[49, 50]. The Bandgap alignment of several III-V materials is shown in Fig. 3(a). Among the III-V materials for fabricating barrier detectors, there is a material system consisting of the near lattice-matched InAs/GaSb/AlSb family of semiconductors—the 6.1 Å material family with room-temperature energy gaps ranging from 0.36 eV (InAs) to 1.61 eV (AlSb)[51]. Fig. 3(b) shows the schematic diagram of the valence band offset as a function of lattice constant[52]. This makes the 6.1 Å lattice-matched family the potential materials for designing the barrier detectors with the desirable unipolar band alignments by adjusting the elemental composition of the compound. Moreover, the bulk GaSb has a direct bandgap in the short-wave IR (SWIR), InAs in the MWIR, and InAs/Ga (In) Sb superlattices in the SWIR, MWIR, and LWIR[53]. The 6.1 Å materials can be epitaxially grown on GaSb and GaAs substrates. In particular, 4-inch diameter GaSb substrates became commercially available in 2009, offering improved economy of scale for fabrication of large format FPAs arrays[48]. At present, the barrier detectors have been successfully applied to the III-V materials system and commercialized.

1.1.1 InAsSb barrier detectors

The InAsSb is an important candidate for fabricating MWIR detectors because of the high carrier mobility, relatively small dielectric constant, and self-diffusion coefficient at room temperature. Due to a nearly zero band valence offset with respect to AlAsSb in the valence band, InAsSb has emerged to play a dominant role in the de-

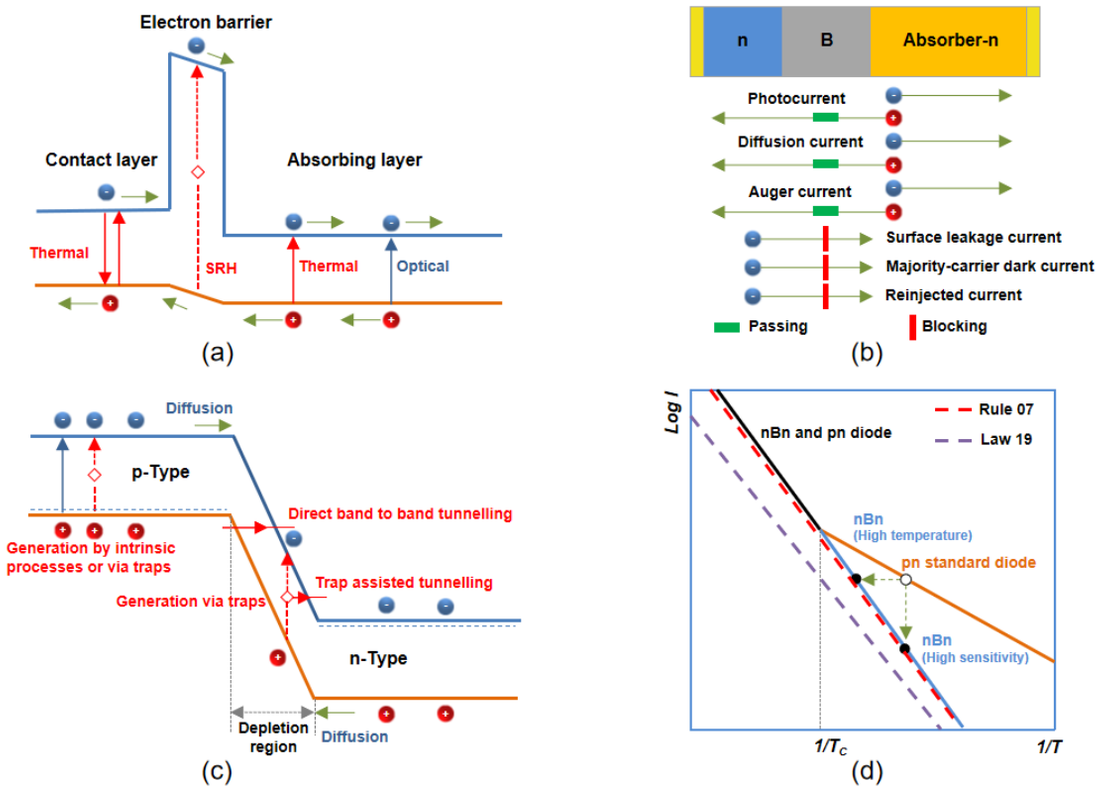

Fig. 2 (a) Bandgap diagram of nBn barrier detector, (b) spatial makeups of the various current components and barrier blocking in nBn detector, (c) bandgap diagram of the p-n photodiode, (d) the schematic Arrhenius plot of the dark current in a p-n photodiode and nBn device and comparision with Rule 07 & Law 19

图2 (a) nBn势垒探测器的能带图,(b)nBn探测器的电流组成成分,(c) p-n结光电二极管的能带图,(d) p-n结光电二极管和nBn器件中的暗电流以及对比Rule 07和Law 19的Arrhenius原理图

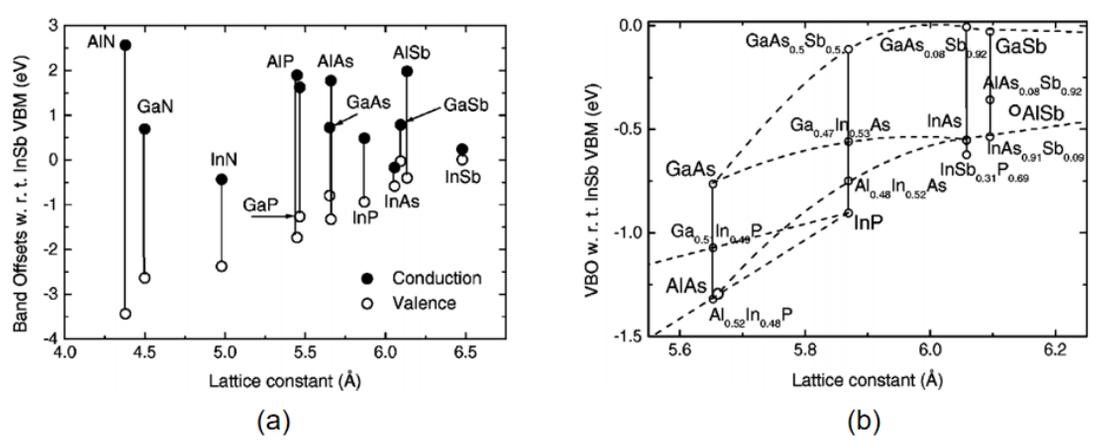

Fig. 3 (a) Conduction (filled) and valence (open) band offsets for the 12 binaries, (b) valence band offset as a function of lattice constant [52]

图3 (a) 12种化合物的导带(实心)和价带(空心)偏移,(b) 价带带阶与晶格常数的关系曲线

signing of the nBn detectors. The InAsSb were grown on either GaAs (100) or GaSb (100) substrates and the n-type doping is usually reached by either Si or Te elements.

Klipstein and Weiss have described the detailed growth procedure and device's characterization of $InAs_{1-x}Sb_x/AlAs_{1-y}Sb_y$ nBn MWIR detector[20, 44]. In 2011, the Klipstein team achieved the InAsSb/AlAsSb nBn detector with a cutoff wavelength of ~4.1 μm and a dark current close to ~3×10^{-7} A/cm^2 at 150 K[54], as shown in Fig. 4(a-b). The device was fabricated nearly lattice-matched to the GaSb substrate, which exists a typical strain of 500 ppm or less. It discussed the cutoff wavelength increases with decreasing absorber layer doping because of the Moss-Burstein effect[55], which blocks interband optical transitions in the absorber layer with final

states in the conduction band that lie below the Fermi energy. Also, the quantum efficiency (*QE*) of the detector is dependent on the thickness of the absorber layer. The FPA detectors with a 320×256 format and 30μm pitch were fabricated which have high operability and a NETD of 16 mK at 150 K, using *f*/3 optics and a 20 ms integration time[44]. By the standard two-point nonuniformity correction procedure of SCD, excellent image quality has been achieved, as shown in Fig. 4(c).

In 2012, D'Souza et al. have demonstrated the nBn detector in the InAsSb/AlAsSb materials system grown by molecular beam epitaxy (MBE) on GaSb and GaAs substrates[56]. The device has a 5 μm cut-off operated at 200 K. The dark current density in the pyramidal structured diodes is reduced by a factor of 2-3, which is consistent with the volume reduction due to pyramid formation. Soibel described InAsSb/AlAsSb nBn detectors with cut-off wavelengths near 4. 5 μm in 2014[57].

The nBn structure is considered theoretically by Martyniuk and Rogalski[58, 59]. The device structure and stimulated energy band diagram are shown in Fig. 4(d-e). Fig. 4(f) shows the I-V characteristics as a function of temperature[60]. The alloy composition x of the $InAs_{1-x}Sb_x$ absorber layer is 0. 195 with a cutoff wavelength of ~ 4. 9 μm at 150 K. And J_{dark} is 1.0×10^{-3} A/cm^2 at 200 K and 3.0×10^{-6} A/cm^2 at 150 K (Fig. 4(f)). The detectors are dominated by diffusion currents at -1 V bias at the *QE* peaks.

Subsequently, Klipstein et al. presented one of the first commercial nBn array detectors operated in the blue part of the MWIR window of the atmosphere (3. 4~4. 2 μm) and launched on the market by SCD in 2014 known as "Kinglet" (640×512, 15 μm), which is the first III-V XBn detector developed by SCD to meet low SWaP applications[50]. The working temperature of the focal plane array is 150 K, the power consumption is 3 W, and the weight is less than 300 g.

HOT Hercules (1280×1024, 15 μm) is SCD's second nBn MW HOT product. It was launched in 2014 and uses the InAsSb material system. The operating temperature of this million-pixels component can reach 150 K[61, 62]. In order to improve the performance of the detector, SCD has also developed the Blackbird series of MWIR digital detectors, the pixel pitch is reduced to 10 μm, with lower power consumption and higher photoelectric performance. The Blackbird series of nBn-InAsSb barrier detectors (1280×1024, 10 μm) have the same photoelectric performance as planar junction InSb detectors, but the working temperature is up to 150 K[63].

1. 1. 2　InSb barrier detectors

InSb is the III-V semiconductor with the narrowest bandgap and the highest electron mobility. InSb IR detectors are intrinsic absorption in the MWIR (3~5 μm) spectral region, as well as extremely high quantum efficiency and responsivity. Therefore, InSb detectors can achieve extremely high thermal sensitivity and excellent image quality, which has become one of the most important MWIR detectors. However, the InSb device has to work at a low temperature of 77 K which greatly restricts its application.

Evirgen et al. first reported the experimental research progress of the InSb IR detector based on the nBn

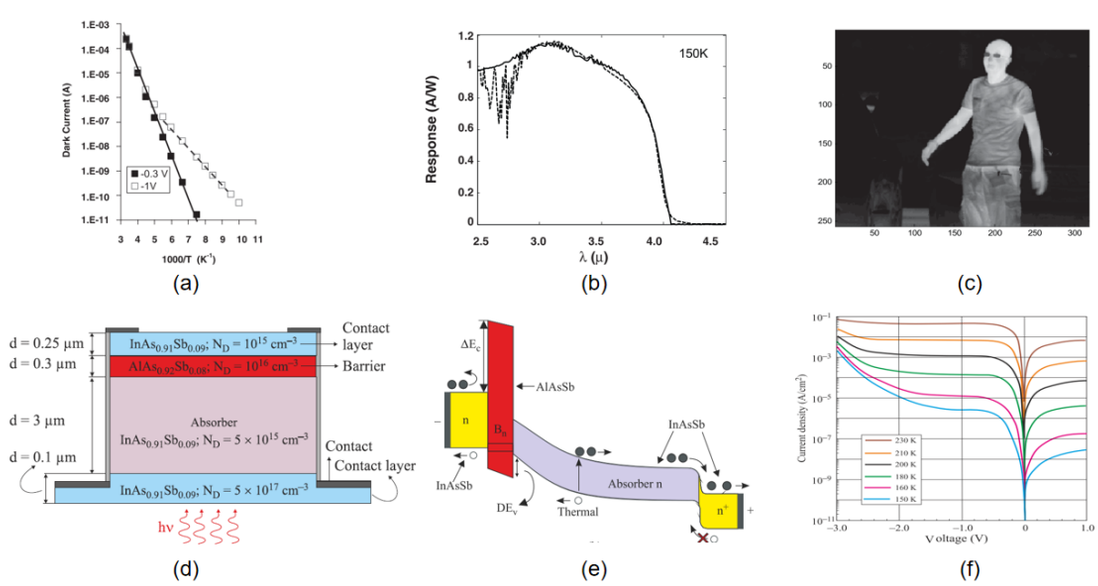

Fig. 4　(a) Arrhenius plot of dark current at different reverse bias values for a 300×300 μm nBn detector, (b) photoresponse spectra at 150 K (the calculated spectral response (solid line) and the measured spectral response at a reverse bias of -0. 6 V (dotted line)), (c) image captured by a 320×256 nBn FPA detector (BF ROIC) operating at 150 K and *f*/3, (d) the device structure of InAsSb/AlAsSb nBn MWIR detector, (e) the stimulated energy band diagram under reverse bias conditions of InAsSb/AlAsSb nBn MWIR detector, (f) the dark current density vs bias voltage as a function of the temperature of the InAsSb/AlAsSb nBn MWIR detector[54, 58, 60]

图 4　(a) 300×300 μm nBn探测器在不同反向偏置下的暗电流 Arrhenius 图, (b) 150 K温度下的光谱响应(理论计算的光谱响应(实线)和在-0. 6 V的反向偏置下测量的光谱响应(虚线)), (c) 由 320×256 nBn FPA 探测器 (BF ROIC) 在 150 K 和 f/3 下工作时捕获的图像, (d) InAsSb/AlAsSb nBn MWIR探测器的器件结构, (e) InAsSb/AlAsSb nBn MWIR探测器反向偏置条件下的能带图, (f) InAsSb/AlAsSb nBn MWIR 探测器的暗电流密度与偏置电压的关系随温度变化的关系曲线

structure in 2014[64]. The structure and energy band of the device are shown in Fig. 5(a-b)[64, 65]. The nBn structure was fabricated by MBE. While the Al-content of the barrier is around 20%, the values of dark current density are easily fitted by current density due to thermionic emission (J_{TE})[5], given by the following equation[66]: $J_{TE}=A^*T^2e^{-\Phi/kT}$, where A^* is Richardson constant including the conduction band effective mass of the n-type contact layer and Φ is the energy difference between the top of the InAlSb barrier and the fermi energy in the contact layer (Fig. 5(c))[64]. It shows that the total current of the device is mainly from the majority electrons of the n-doped InSb cap layer. In order to achieve a sufficiently high conduction band barrier to block electrons while maintaining a lower valence band barrier to allow the flow of photo-generated holes, the barrier layer of the device adopts a graded Al composition design. The dark current of InSb nBn detector reaches 1×10^{-9} A/cm^2 under 77 K and -50 mV bias (Fig. 5(d)), which is 2×10^{-5} A/cm^2 under 135 K and -50 mV bias (Fig. 5(e))[65].

As shown in Fig. 5(f), compared with the InSb PIN detector fabricated by MBE and standard planar process of SOFRADIR, the dark current of nBn device is significantly suppressed. The nBn detector can operate at a temperature of around 120 K, which is 20 K higher than the PIN device and 40 K higher than the standard planar process[67]. Such a result demonstrates the potentiality of the application of the InSb nBn detector.

In addition, the DAT-CON company of Slovenia has developed MWIR FPA based on XBn-InSb detectors, including the CLRT series (640×512, 15 μm) and CLRT HD series (1280×1024, 10 μm). The detective spectral range is 3.4~5.1 μm and NETD reaches 25 mK[20].

1.1.3 T2SLs barrier detectors

The type-II superlattice material has become the focus of the development of the third generation of infrared detectors for its inherent lower Auger G-R rate, large effective mass of electrons (small tunneling current between bands, small dark current), adjustable energy band, and good uniformity. From the perspective of the T2SLs structure, the electrons and holes are spatially separated and localized in self-consistent quantum wells formed on both sides of the heterointerface[37]. The unique "broken bandgap" energy band structure enables T2SLs IR detectors to achieve higher device performance and operating temperature in MW/LW IR detection. In addition, the advantage of T2SLs for IR detectors is the property to tune the wavelength by adjusting one of the material components and fixing the other[68], which is especially crucial in the design of nBn detectors.

InAs/GaSb heterojunctions were found by Sakaki in 1977, which are generally considered to be a material that can replace the current mainstream HgCdTe with its unique characteristics[69]. In the InAs/GaSb T2SLs system, the AlAsSb barrier layer is generally used to fabricate the nBn detector, owing to the InAs/GaSb T2SLs having an almost zero valence band offset relative to the AlAsSb barrier[48].

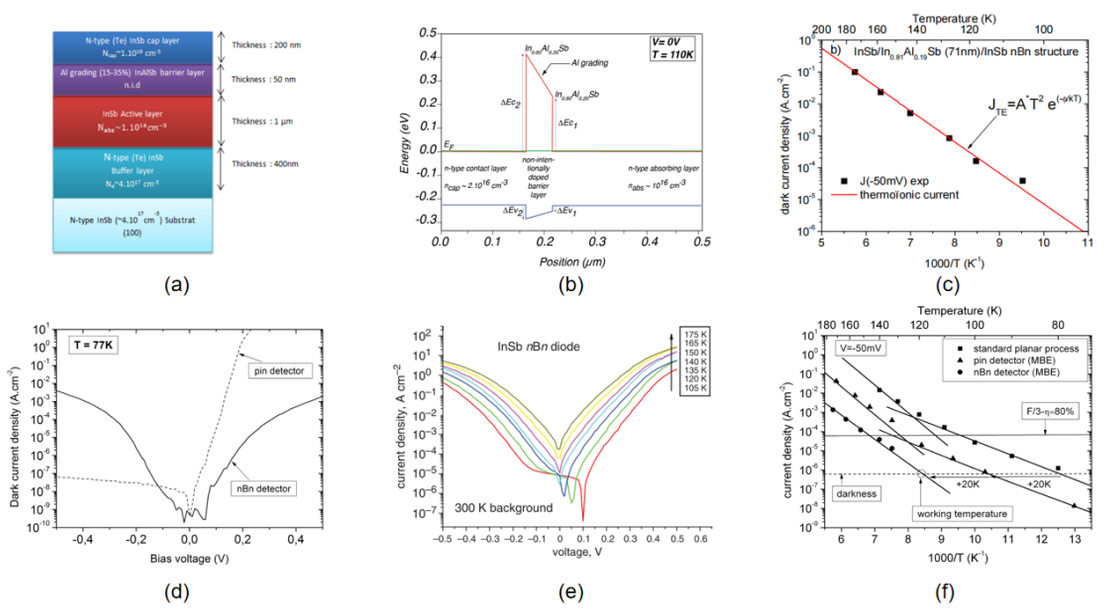

Fig. 5 Design of the InSb nBn barrier detector, (a) design of InSb nBn structure with InAlSb barrier layer including Al grading from 15% to 35%, (b) calculated energy band diagram at T = 110 K and V = 0 V of InSb/InAlSb/InSb nBn structure with 50 nm-thick InAlSb graded composition barrier layer, (c) Arrhenius plot of the dark current density collected at -50 mV where thermionic emission regime is identified, (d) *J-V* curves performed at 77 K of InSb-based nBn detector (solid line) and InSb PIN diode (dashed line), (e) *J-V* characteristics of nBn structure for different operating temperatures, from 105 K to 175 K, (f) Arrhenius behavior of three different types of InSb-based photodetectors[64, 65, 67]

图5 InSb nBn势垒探测器的设计(a) InSb nBn器件结构设计图,阻挡层为Al组15%至35%渐变的InAlSb,(b) 具有50 nm渐变组分InAlSb势垒层的InSb/InAlSb/InSb nBn结构在T = 110 K和V = 0 V时的理论计算的能带图,(c) 在-50 mV偏压下的暗电流密度的Arrhenius图,其中确定了热电子发射状态,(d) 基于InSb的nBn探测器(实线)和InSb PIN二极管(虚线)在77 K下的J-V曲线,(e) 105 K到175 K不同工作温度下nBn结构的J-V特性,(f) 三种不同类型的基于InSb的光电探测器Arrhenius图

Rodriguez in the university of New Mexico applied the nBn structure to the T2SLs detector for the first time in 2007[70]. In 2015, SCD presented the long-wave FPA "Pelican-D LW" (640×512, 15 μm) using the pBp structure, which is the first LW FPA product of SCD[71]. The absorber layer and electrode layer of the device are InAs/GaSb T2SLs, while the barrier layer is InAs/AlSb T2SLs. The alignment between mini-bands is shown in Fig. 6(a). The operating temperature of the detector is 77 K, and the cut-off wavelength is 9.5 μm. The dark current is as low as 4.4×10^{-5} A/cm^2 at 77 K.

Northwestern University reported a short-wave T2SLs photodetector based on the nBn structure in 2017[72]. The device was fabricated on GaSb substrate based on InAs/AlSb/GaSb T2SLs, and $AlAs_{0.1}Sb_{0.9}$/GaSb H-structure SL design was used as the large bandgap electron barrier (Fig. 6(b)). The photodetector has a peak responsivity of 0.65 A/W at room temperature at 1.9 μm. At 300 K and 400 mV bias, the dark current density is 8×10^{-3} A/cm^2 and the D^* is 1.51×10^{10} cm·Hz$^{1/2}$W^{-1}. At 150 K, the dark current density is 9.5×10^{10} A/cm^2, the quantum efficiency is 50%, and the D^* is 1.12×10^{13} cm·Hz$^{1/2}$W^{-1}.

The T2SLs IR detectors have developed rapidly in the past 10 years. The focus of future research is on the device structure design and FPA technology. The barrier device structure is expected to further reduce the dark current of the device and enhance the performance.

1.2 MCT barrier detectors

In 1959, Lawson invented the direct bandgap ternary compound semiconductor material with continuously adjustable bandgap width—$Hg_{1-x}Cd_xTe$[1]. By changing the component x, the bandgap width meets the infrared detection of three atmospheric windows of 1~3 μm, 3~5 μm, and 8~14 μm. Meanwhile, there is an absolutely small change of lattice constant with component x making it possible to grow high-quality heterostructures. The advantages of the high quantum efficiency of the HgCdTe material make it a key core IR device that is widely used in the optoelectronic system of military equipment[73, 74]. However, there are several drawbacks associated with HgCdTe photodetectors. Firstly, the weak ionic Hg-Te bonds and high Hg vapor pressure make the epitaxial growth is more challenging than typical III-V compounds. In addition, HgCdTe is easy to oxidize in the air for its unstable physical and chemical properties.

Considering the successful application of nBn barrier detectors for III-V materials, it is expected to be introduced into HgCdTe materials to overcome the processing technology limitations of typical p-n junctions. However, the implementation of nBn structure in the HgCdTe material is not ideal due to the existence of non-zero valence band offset at the absorber – barrier interface which enormously limits their performance[43, 75]. At low bias, the valence band barrier (ΔE_v) inhibits the holes flow to the contact cap layer as a result the devices always exhibit lower sensitivity and detectivity. In order to align the valance band, a high operating bias—"turn-on" voltage, typically greater than the bandgap energy is required depending on the operating wavelength, which leads to strong band-to-band and trap-assisted tunneling due to high electric field within the depletion layer[68].

Itsuno et al[30, 76, 77]. and Kopytko et al[78]. introduced the nBn structure to HgCdTe for the first time and performed theoretical simulation calculations on the device. The band structure is shown in Fig. 7(a). Compared with the p-n junction structure, the nBn structure presents tight dark current density, responsivity, and detectivity at a temperature from 50 K to 95 K and it shows that the HgCdTe unipolar barrier device based on the nBn structure is very promising for the MWIR and LWIR detection. Thereafter, the research group realized the fabrication of HgCdTe nBn devices. The material parameters are shown in Fig. 7(b). The dark current is saturated with a reverse bias of approximately -0.8 V shown in Fig. 7(c) and a cut-off wavelength of approximately 5.7 μm is observed[76]. Subsequently, the results of HgCdTe devices based on the nBn structure and optimization have been reported successively internationally.

In 2020, Voitsekhovskii et al. presented an MWIR

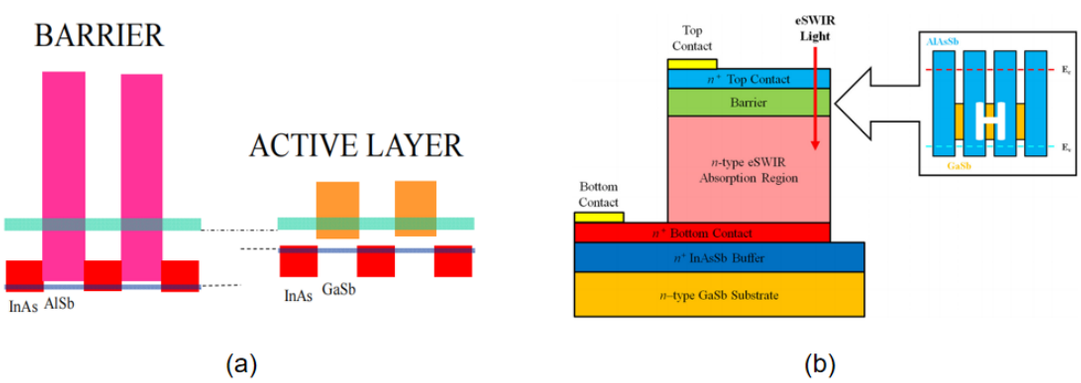

Fig. 6 (a) Alignment between mini-bands in the active and barrier layers of a T2SLs XBp device, superimposed on the band gaps of InAs, GaSb, and AlSb, (b) the schematic diagram of the SWIR nBn photodetector with the inset showing the superlattice band alignment of the H-structure electron barrier[71, 72]

图6 (a) T2SLs XBp器件的有源层和势垒层中的微带位置,(b) SWIR nBn光电探测器示意图(插图为H结构电子势垒的超晶格能带位置)

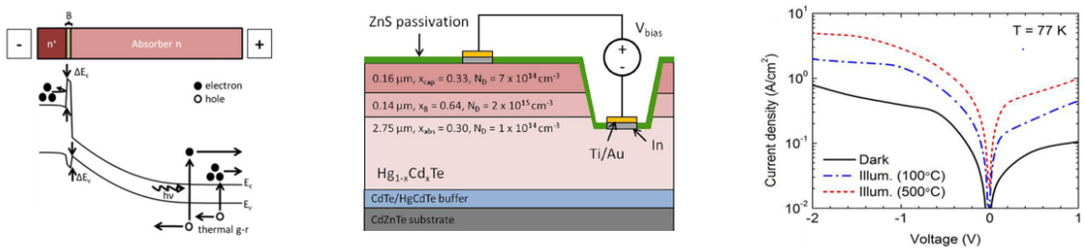

Fig. 7 Design of the HgCdTe nBn barrier detector, (a) the schematic illustration of the structure of the HgCdTe nBn photodetector device, (b) cross-sectional device diagram and structural parameters, (c) measured dark and unfiltered blackbody illuminated *I-V* characteristics of planar MWIR HgCdTe nBn device at 77 K[30, 79]

图7 HgCdTe nBn势垒探测器的设计 (a) HgCdTe nBn光电探测器的能带结构示意图,(b) 器件截面图和结构参数,(c) 77 K下测试的平面MWIR HgCdTe nBn器件的暗态和黑体照射的I-V特性

HgCdTe nBn detector grown by MBE on GaAs substrate[80]. To further suppress the surface current, there is passivation of the Al_2O_3 layer grown by plasma-enhanced atomic layer deposition (PE-ALD). The dark current density of the detector is 3.1×10^{-6} A/cm^2 at 184 K and has a bias of -1 V.

At present, although the application prospects of nBn HgCdTe photodetectors have been extensively explored, their research is mostly at the theoretical stage. The application of nBn architecture to HgCdTe presents a serious challenge due to the difficulty of achieving an ideal nBn band structure which has a zero valence band. The existence of a valence band offset seriously limits the device performance[81]. Present strategy in the development of HgCdTe nBn detectors concentrates on decreasing or even removing the ΔE_v in the barrier layer, which will make it have lower operating bias, lower dark current, and operate at higher temperatures. There are several ways being proposed to eliminate valence band offset, such as composition optimization and doping modulation technique of barrier layer[82-84] and superlattice barrier layer[85, 86]. The appropriate p-type doping of the barrier layer can reduce ΔE_v and increase the ΔE_c. According to previous reports, by applying the barrier layer based on the Type III CdTe/HgTe superlattice structure replacing the single-layer barrier structure, the ideal energy band structure can be obtained by adjusting the thickness and doping of the CdTe and HgTe layers[85]. To a certain extent, it is worth noting that barrier detectors are the most promising approach to achieve HgCdTe detectors operating at close to room temperature. Table 1 is the nBn infrared detector products that have been launched.

1.3 Two-dimensional material barrier detectors

Considering the strict requirements of lattice and band matching of designing nBn barrier detectors with

Table 1 Development status of nBn infrared detectors[87-93]
表1 nBn红外探测器的发展概况[87-93]

Organization	Material	Structure	Size	Pixel size (μm)	Spectral range (μm)	Temperature (K)	NETD (mK)
Northwestern University	InAs/AlSb/GaSb	nBn	1280×1024	12	2.22	150	–
	T2SL	pMp	320×256	27	4.9	150	11
JPL	InAs/InAsSb	BIRD	640×512	24	5.4	150	18.7
	InAs/InAsSb	BIRD	640×512	24	12.5	62	16.3
SCD	InAsSb	nBn	640×512	15	3.6~4.2	150	<25
	InAsSb	nBn	1280×1024	15	3.4~4.2	150	<25
	InAsSb	nBn	1280×1024	10	–	150	30
	InAs/GaSb T2SL	pBp	640×512	15	9.5	80	15
Wuhan Guide	T2SL	npn	320×256	30	4.8/9.5	80	20/25
	T2SL	p×Ma	320×256	30	9.5	–	25
	T2SL	p×Mn	640×512	15	9.5	–	25
SITP	InAs/GaSb T2SL	npn	640×512	30	4.5/5.8	–	–
	InAs/GaAsSb T2SL	pB×Bn	320×256	30	11	80	21
DAT-CON	InSb	XBn	640×512	15	–	–	23
	InSb	XBn	1280×1024	10	–	–	25

conventional materials is extremely challenging. Two-dimensional materials are innovated to fabricate nBn detectors for their self-passivated surfaces, tunable band structures, and avoidable lattice mismatch and interface defects. The ultra-thin and atomic-level flat ideal interface of 2D materials provides the possibility for designing high-performance heterojunction devices. Recently, Hu et al. have presented a nBn unipolar barrier photodetectors based on a tungsten disulfide/hexagonal boron nitride/palladium diselenide (WS_2/h-BN/$PdSe_2$) heterostructure in which WS_2 is used as a visible-wavelength n-type photon absorber, h-BN as the barrier and $PdSe_2$ as the contract layer[94]. The structure of the device is shown in Fig. 8(a). 2D materials are prepared by the mechanical peeling method, and through non-destructive fixed-point transfer, a heterojunction without lattice mismatch and thermal mismatch is obtained.

The band structure achieved from simulation analysis using Sentaurus-TCAD is illustrated in Fig. 8(b) with drain biases ranging from 0 V to -0.5 V. It can be seen from the simulation results that there is an obvious electronic barrier in the conduction band. From the output characteristic curves under 520 nm laser illumination depicted in Fig. 8(c), the nBn photodetector exhibits a dark current of the order of pA, a photocurrent of 20 μA. Under the room temperature at 520 nm, the detectivity of the device reaches up to 2.7×10^{12} cm·$Hz^{1/2}W^{-1}$.

The barrier photodetectors based on 2D material are currently in the initial research stage, and there are no other relevant literature reports. The above-mentioned research results will create a foundation for subsequent research. Therefore, the barrier photodetectors fabricated by 2D material could have good prospects in IR photoelectric detection.

2 Conclusion and outlook

The efforts in IR detection technology particularly aim to increase the operating temperature reaching the HOT demand[7]. A relatively novel nBn structure based on a unipolar barrier has materials and thus enhances the operating temperature because it is not limited by G-R current and tunneling currents. Research based on various material systems mentioned above shows that the barrier structure has great potential.

Significant effort has been devoted to developing nBn barrier detectors based on the III-V materials. Up to now, nBn barrier detectors based on III-V materials (InAsSb, InAs/GaSb T2SLs, et al.) have been successfully industrialized, and the performance of the devices has also been greatly improved. Among these, III-V T2SLs materials, such as InAs/GaSb and InAs/InAsSb, are considered to be the most promising competitor to HgCdTe IR detectors. However, T2SLs IR detectors suffer from a major limitation related to the short SRH carrier lifetime (<100 ns experimentally). Although the intensive research effort has been devoted over the last decade, little improvement has been acquired. Compare with the state-of-the-art HgCdTe detectors, its performance advantage is not significant mainly due to the lower quantum efficiency and shorter minority carrier lifetime limited by SRH GR mechanisms. However, it appears that T2SLs are especially potential in the design of barrier detectors because of the ability to tune the wavelength by adjusting one of the material components and fixing the other. What's more, the high quality, high uniformity of fabricated FPAs of T2SLs material system is very suitable for today's application needs and in an early stage of development which reached rapid progress in recent years, it will have a great promise in the design of nBn barrier detectors for the future IR solutions.

In recent years, new low-dimensional materials are progressing rapidly in material growth, device fabrication, and characterization. At the same time, the production of 2D-materials heterojunctions can avoid the limitation of lattice matching of the traditional heterojunction interface, thereby realizing more optoelectronic devices with new functions, high sensitivity, and room temperature IR detection. Therefore, combing the traditional bulk materials with excellent photoelectric properties with low-dimensional materials, it is effective to optimize the heterojunction interface and avoid the complex fabrication process and large interface damage of traditional bulk materials.

The nBn barrier structure based on energy band en-

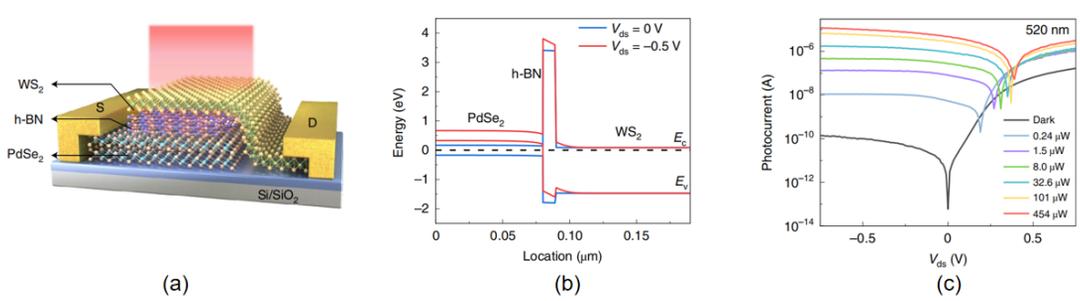

Fig. 8　Design of the two-dimensional materials nBn barrier detector, (a) the schematic diagram of the WS_2 nBn vdW unipolar barrier photodetector, (b) simulated band diagrams of the device under different source-drain bias (V_{ds}) conditions (WS_2, h-BN, and $PdSe_2$ flakes act as the absorber, barrier, and contact layer, respectively), (c) output characteristic curves of the nBn vdW unipolar barrier device under 520 nm laser illumination with increasing powers[94]

图 8　二维材料 nBn 势垒探测器的设计 (a) WS2 nBn vdW 单极势垒光电探测器的示意图,(b) 不同源漏偏压 (Vds) 条件下器件的模拟能带图(WS2、h-BN 和 PdSe2 分别为吸收层、阻挡层和接触层),(c) nBn vdW 单极势垒器件在 520 nm 激光照射下的变功率输出特性曲线

gineering has continuously made breakthroughs in low dark current and high operating temperature. This new IR detector structure with strategically important technology is expected to lead to the further development of a new generation of infrared detection technology.

References

[1] Rogalski A. Infrared and Terahertz Detectors [M]. Third Edition: CRC Press, 2019.

[2] Rogalski A. History of infrared detectors [J]. *Opto-Electronics Review*, 2012, **20**(3): 279-308.

[3] Bürsing H, Ebert R, Huckridge D A, *et al*. Next decade in infrared detectors [J]. 2017: 100.

[4] Corsi C. History highlights and future trends of infrared sensors [J]. *Journal of Modern Optics*, 2010, **57**(18): 1663-1686.

[5] Manissadjian A, Rubaldo L, Rebeil Y, *et al*. Improved IR detectors to swap heavy systems for SWaP[C].Infrared Technology and Applications XXXVIII. International Society for Optics and Photonics, 2012, **8353**: 835334.

[6] Driggers R, Vollmerhausen R, Reynolds J, *et al*. Infrared detector size: how low should you go? [J]. *Optical Engineering*, 2012, **51**(6): 063202.

[7] Rogalski A, Martyniuk P, Kopytko M. Challenges of small-pixel infrared detectors: a review [J]. *Rep Prog Phys*, 2016, **79**(4): 046501.

[8] Rogalski A, Razeghi M. Narrow-gap semiconductor photodiodes[C]. Photodetectors: Materials and Devices III. International Society for Optics and Photonics, 1998, **3287**: 2-13.

[9] Ashley T, Elliott C T. Nonequilibrium devices for infra-red detection [J]. *Electronics Letters*, 1985, **21**(10): 451-452.

[10] Gendron L, Carras M, Huynh A, *et al*. Quantum cascade photodetector [J]. *Applied Physics Letters*, 2004, **85**(14): 2824-2826.

[11] Li J V, Yang R Q, Hill C J, *et al*. Interband cascade detectors with room temperature photovoltaic operation [J]. *Applied Physics Letters*, 2005, **86**(10).

[12] Smith D L, Mailhiot C. Proposal for strained type II superlattice infrared detectors [J]. *Journal of Applied Physics*, 1987, **62**(6): 2545-2548.

[13] Maimon S, Wicks G W. nBn detector, an infrared detector with reduced dark current and higher operating temperature [J]. *Applied Physics Letters*, 2006, **89**(15).

[14] Maimon S, Wicks G W. nBn detector, an infrared detector with reduced dark current and higher operating temperature [J]. *Applied Physics Letters*, 2006, **89**(15): 151109.

[15] Razeghi M, Tournié E, Brown G J, *et al*. InSb photodetectors with PIN and nBn designs [J]. 2013, **8993**: 899313.

[16] Evirgen A, Perez J P, Christol P, *et al*. Midwave infrared InSb nBn photodetector [J]. *Electronics Letters*, 2014, **50**(20): 1472-1473.

[17] Perez J P, Evirgen A, Abautret J, *et al*. MWIR InSb detector with nBn architecture for high operating temperature [C]. Quantum Sensing and Nanophotonic Devices XII. International Society for Optics and Photonics, 2015, **9370**: 93700N.

[18] Klipstein P. " XBn" barrier photodetectors for high sensitivity and high operating temperature infrared sensors [C]. Infrared Technology and Applications XXXIV. International Society for Optics and Photonics, 2008, **6940**: 69402U.

[19] Khoshakhlagh A, Myers S, Plis E, *et al*. Mid-wavelength InAsSb detectors based on nBn design [C]. Infrared Technology and Applications XXXVI. International Society for Optics and Photonics, 2010, **7660**: 76602Z.

[20] Weiss E, Klin O, Grossmann S, *et al*. InAsSb-based XBnn bariodes grown by molecular beam epitaxy on GaAs [J]. *Journal of Crystal Growth*, 2012, **339**(1): 31-35.

[21] Soibel A, Hill C J, Keo S A, *et al*. Room temperature performance of mid-wavelength infrared InAsSb nBn detectors [J]. *Applied Physics Letters*, 2014, **105**(2): 023512.

[22] Rodriguez J B, Plis E, Bishop G, *et al*. nBn structure based on InAs/GaSb type-II strained layer superlattices [J]. *Applied Physics Letters*, 2007, **91**(4): 043514.

[23] Ting D Z, Hill C J, Soibel A, *et al*. Antimonide-based barrier infrared detectors [C]//Infrared Technology and Applications XXXVI. International Society for Optics and Photonics, 2010, **7660**: 76601R.

[24] Khoshakhlagh A, Myers S, HaSul K, *et al*. Long-Wave InAs/GaSb Superlattice Detectors Based on nBn and Pin Designs [J]. *IEEE Journal of Quantum Electronics*, 2010, **46**(6): 959-964.

[25] Kim H S, Cellek O O, Lin Z-Y, *et al*. Long-wave infrared nBn photodetectors based on InAs/InAsSb type-II superlattices [J]. *Applied Physics Letters*, 2012, **101**(16): 161114.

[26] Ting D Z, Soibel A, Khoshakhlagh A, *et al*. Antimonide type-II superlattice barrier infrared detectors [C].Infrared Technology and Applications Xliii. International Society for Optics and Photonics, 2017, **10177**: 101770N.

[27] Haddadi A, Chevallier R, Dehzangi A, *et al*. Extended short-wavelength infrared nBn photodetectors based on type-II InAs/AlSb/GaSb superlattices with an AlAsSb/GaSb superlattice barrier [J]. *Applied Physics Letters*, 2017, **110**(10): 101104.

[28] Rhiger D R, Smith E P. Carrier Transport in the Valence Band of nBn III - V Superlattice Infrared Detectors [J]. *Journal of Electronic Materials*, 2019, **48**(10): 6053-6062.

[29] Ting D Z, Soibel A, Khoshakhlagh A, *et al*. Development of InAs/InAsSb Type II Strained-Layer Superlattice Unipolar Barrier Infrared Detectors [J]. *Journal of Electronic Materials*, 2019, **48**(10): 6145-6151.

[30] Itsuno A M, Phillips J D, Velicu S. Design and Modeling of HgCdTe nBn Detectors [J]. *Journal of Electronic Materials*, 2011, **40**(8): 1624-1629.

[31] Itsuno A M, Phillips J D, Velicu S. Design of an Auger-Suppressed Unipolar HgCdTe NBνN Photodetector [J]. *Journal of Electronic Materials*, 2012, **41**(10): 2886-2892.

[32] Itsuno A M, Phillips J D, Velicu S. Mid-wave infrared HgCdTe nBn photodetector [J]. *Applied Physics Letters*, 2012, **100**(16): 161102.

[33] Akhavan N D, Umana-Membreno G A, Jolley G, *et al*. A method of removing the valence band discontinuity in HgCdTe-based nBn detectors [J]. *Applied Physics Letters*, 2014, **105**(12): 121110.

[34] Kopytko M. Design and modelling of high-operating temperature MWIR HgCdTe nBn detector with n- and p-type barriers [J]. *Infrared Physics & Technology*, 2014, **64**: 47-55.

[35] Gravrand O, Boulard F, Ferron A, *et al*. A New nBn IR Detection Concept Using HgCdTe Material [J]. *Journal of Electronic Materials*, 2015, **44**(9): 3069-3075.

[36] Savich G R, Pedrazzani J R, Sidor D E, *et al*. Dark current filtering in unipolar barrier infrared detectors [J]. *Applied Physics Letters*, 2011, **99**(12): 121112.

[37] Martyniuk P, Kopytko M, Rogalski A. Barrier infrared detectors [J]. *Opto-Electronics Review*, 2014, **22**(2): 127-146.

[38] Kazemi A, Myers S, Taghipour Z, *et al*. Mid-wavelength infrared unipolar nBp superlattice photodetector [J]. *Infrared Physics & Technology*, 2018, **88**: 114-118.

[39] Uzgur F, Kocaman S. Barrier engineering for HgCdTe unipolar detectors on alternative substrates [J]. *Infrared Physics & Technology*, 2019, **97**: 123-128.

[40] Vallone M, Goano M, Bertazzi F, *et al*. Constraints and performance trade-offs in Auger-suppressed HgCdTe focal plane arrays [J]. *Appl Opt*, 2020, **59**(17): E1-E8.

[41] Vallone M, Goano M, Bertazzi F, *et al*. Reducing inter-pixel crosstalk in HgCdTe detectors [J]. *Optical and Quantum Electronics*, 2019, **52**(1).

[42] Sah C T, Noyce R N, Shockley W. Carrier generation and recombination in pn junctions and pn junction characteristics [J]. *Proceedings of the IRE*, 1957, **45**(9): 1228-1243.

[43] Savich G R, Pedrazzani J R, Sidor D E, *et al*. Benefits and limitations of unipolar barriers in infrared photodetectors [J]. *Infrared Physics & Technology*, 2013, **59**: 152-155.

[44] Klipstein P. "XBn " barrier photodetectors for high sensitivity and high operating temperature infrared sensors [J]. *Proc of SPIE Vol 6940 69402U-1*, 2008.

[45] Tennant W E, Lee D, Zandian M, *et al*. MBE HgCdTe Technology: A Very General Solution to IR Detection, Described by "Rule 07", a Very Convenient Heuristic [J]. *Journal of Electronic Materials*, 2008, **37**(9): 1406-1410.

[46] Lee D, Dreiske P, Ellsworth J, *et al*. Law 19: The ultimate photodiode performance metric [C]//Infrared Technology and Applications XLVI. International Society for Optics and Photonics, 2020, **11407**: 114070X.

[47] Savich G R, Sidor D E, Du X, *et al*. Diffusion current characteristics of defect-limited nBn mid-wave infrared detectors [J]. *Applied Physics Letters*, 2015, **106**(17): 173505.

[48] Rogalski A, Martyniuk P. Mid-Wavelength Infrared nBn for HOT Detectors [J]. *Journal of Electronic Materials*, 2014, **43**(8): 2963-

2969.
[49] Klipstein P, Klin O, Grossman S, *et al*. High operating temperature XBn-InAsSb bariode detectors[C].Quantum Sensing and Nanophotonic Devices IX. International Society for Optics and Photonics, 2012, **8268**: 82680U.
[50] Klipstein P C, Gross Y, Aronov D, *et al*. Low SWaP MWIR detector based on XBn focal plane array[C].Infrared Technology and Applications XXXIX. International Society for Optics and Photonics, 2013, **8704**: 87041S.
[51] Kroemer H. The family (InAs, GaSb, AlSb) and its heterostructures: a selective review [J]. *Physica E: Low-dimensional Systems and Nanostructures*, 2004, **20**(3-4): 196-203.
[52] Vurgaftman I, Meyer J R, Ram-Mohan L R. Band parameters for III – V compound semiconductors and their alloys [J]. *Journal of Applied Physics*, 2001, **89**(11): 5815-5875.
[53] Ting D Z, Hill C J, Soibel A, *et al*. Antimonide-based barrier infrared detectors[C]//Infrared Technology and Applications XXXVI. International Society for Optics and Photonics, 2010, **7660**: 76601R.
[54] Klipstein P. XBn barrier photodetectors based on InAsSb with high operating temperatures [J]. *Optical Engineering*, 2011, **50**(6).
[55] Klipstein P, Klin O, Grossman S, *et al*. XBn barrier detectors for high operating temperatures[C].Quantum Sensing and Nanophotonic Devices VII. International Society for Optics and Photonics, 2010, **7608**: 76081V.
[56] D′Souza A I, Robinson E, Ionescu A C, *et al*. MWIR InAs1-xSbx nCBn detectors data and analysis[C].Infrared Technology and Applications XXXVIII. International Society for Optics and Photonics, 2012, **8353**: 835333.
[57] Soibel A, Hill C J, Keo S A, *et al*. Room temperature performance of mid-wavelength infrared InAsSb nBn detectors [J]. *Applied Physics Letters*, 2014, **105**(2).
[58] Martyniuk P, Rogalski A. Modeling of InAsSb/AlAsSb nBn HOT detector′s performance limit[C]//Infrared Technology and Applications XXXIX. International Society for Optics and Photonics, 2013, **8704**: 87041X.
[59] Martyniuk P, Rogalski A. Performance limits of the mid-wave InAsSb/AlAsSb nBn HOT infrared detector [J]. *Optical and Quantum Electronics*, 2013, **46**(4): 581-591.
[60] D′Souza A I, Robinson E, Ionescu A C, *et al*. MWIR InAsSb barrier detector data and analysis[C].Infrared Technology and Applications XXXIX. International Society for Optics and Photonics, 2013, **8704**: 87041V.
[61] Karni Y, Avnon E, Ezra M B, *et al*. Large format 15μm pitch XBn detector[C]//Infrared Technology and Applications XL. International Society for Optics and Photonics, 2014, **9070**: 90701F.
[62] Klipstein P, Klin O, Grossman S, *et al*. MWIR InAsSb XB_n detector (bariode) arrays operating at 150K[C].Infrared Technology and Applications XXXVII. International Society for Optics and Photonics, 2011, **8012**: 80122R.
[63] Gershon G, Avnon E, Brumer M, *et al*. 10 μm pitch family of InSb and XBn detectors for MWIR imaging[C].Infrared Technology and Applications XLIII. International Society for Optics and Photonics, 2017, **10177**: 101771I.
[64] Evirgen A, Abautret J, Perez J P, *et al*. InSb photodetectors with PIN and nBn designs[C].Quantum Sensing and Nanophotonic Devices XI. International Society for Optics and Photonics, 2014, **8993**: 899313.
[65] Evirgen A, Abautret J, Perez J P, *et al*. Midwave infrared InSb nBn photodetector [J]. *Electronics Letters*, 2014, **50**(20): 1472-1473.
[66] Sze S M, Li Y, Ng K K. Physics of semiconductor devices[M]. John wiley & sons, 2021.
[67] Perez J P, Evirgen A, Abautret J, *et al*. MWIR InSb detector with nBn architecture for high operating temperature[C]//Quantum Sensing and Nanophotonic Devices XII. International Society for Optics and Photonics, 2015, **9370**: 93700N.
[68] Rogalski A, Martyniuk P, Kopytko M. Type-II superlattice photodetectors versus HgCdTe photodiodes [J]. *Progress in Quantum Electronics*, 2019, 68.
[69] Sakaki H, Chang L L, Ludeke R, *et al*. $In_{1-x}Ga_xAs$-$GaSb_{1-y}As_y$ heterojunctions by molecular beam epitaxy [J]. *Applied Physics Letters*, 1977, **31**(3): 211-213.
[70] Rodriguez J B, Plis E, Bishop G, *et al*. nBn structure based on InAs/GaSb type-II strained layer superlattices [J]. *Applied Physics Letters*, 2007, **91**(4).
[71] Klipstein P C, Avnon E, Benny Y, *et al*. Type-II superlattice detector for long-wave infrared imaging[C].Infrared Technology and Applications XLI. International Society for Optics and Photonics, 2015, **9451**: 94510K.
[72] Haddadi A, Chevallier R, Dehzangi A, *et al*. Extended short-wavelength infrared nBn photodetectors based on type-II InAs/AlSb/GaSb superlattices with an AlAsSb/GaSb superlattice barrier [J]. *Applied Physics Letters*, 2017, **110**(10): 101104.
[73] Hu W, Ye Z, Liao L, *et al*. 128 × 128 long-wavelength/mid-wavelength two-color HgCdTe infrared focal plane array detector with ultralow spectral cross talk [J]. *Optics Letters*, 2014, **39**(17): 5184-5187.
[74] Hu W D, Chen X S, Ye Z H, *et al*. A hybrid surface passivation on HgCdTe long wave infrared detector with in-situ CdTe deposition and high-density hydrogen plasma modification [J]. *Applied Physics Letters*, 2011, **99**(9): 091101.
[75] Savich G R, Pedrazzani J R, Sidor D E, *et al*. Use of unipolar barriers to block dark currents in infrared detectors[C].Infrared Technology and Applications XXXVII. International Society for Optics and Photonics, 2011, **8012**: 80122T.
[76] Kim H S, Cellek O O, Lin Z-Y, *et al*. Long-wave infrared nBn photodetectors based on InAs/InAsSb type-II superlattices [J]. *Applied Physics Letters*, 2012, **101**(16).
[77] Velicu S, Zhao J, Morley M, *et al*. Theoretical and experimental investigation of MWIR HgCdTe nBn detectors[C]. Quantum Sensing and Nanophotonic Devices IX. International Society for Optics and Photonics, 2012, **8268**: 82682X.
[78] Kopytko M, Kębłowski A, Gawron W, *et al*. High-operating temperature MWIR nBn HgCdTe detector grown by MOCVD[J]. *Opto-Electronics Review*, 2013, **21**(4): 402-405.
[79] Itsuno A M, Phillips J D, Velicu S. Mid-wave infrared HgCdTe nBn photodetector [J]. *Applied Physics Letters*, 2012, **100**(16).
[80] Voitsekhovskii A V, Nesmelov S N, Dzyadukh S M, *et al*. Diffusion-limited dark currents in mid-wave infrared HgCdTe-based nBn structures with Al_2O_3 passivation[J]. *Journal of Physics D: Applied Physics*, 2019, **53**(5): 055107.
[81] Akhavan N D, Jolley G, Umana-Membreno G A, *et al*. Theoretical study of midwave infrared HgCdTe nBn detectors operating at elevated temperatures[J]. *Journal of Electronic Materials*, 2015, **44**(9): 3044-3055.
[82] Akhavan N D, Jolley G, Umana-Membreno G A, *et al*. Performance Modeling of Bandgap Engineered HgCdTe-Based nBn Infrared Detectors [J]. *IEEE Transactions on Electron Devices*, 2014, **61**(11): 3691-3698.
[83] Akhavan N D, Umana-Membreno G A, Jolley G, *et al*. A method of removing the valence band discontinuity in HgCdTe-based nBn detectors [J]. *Applied Physics Letters*, 2014, **105**(12).
[84] Akhavan N D, Umana-Membreno G A, Gu R, *et al*. Delta Doping in HgCdTe-Based Unipolar Barrier Photodetectors [J]. *IEEE Transactions on Electron Devices*, 2018, **65**(10): 4340-4345.
[85] Kopytko M, Wróbel J, Jóźwikowski K, *et al*. Engineering the Bandgap of Unipolar HgCdTe-Based nBn Infrared Photodetectors [J]. *Journal of Electronic Materials*, 2014, **44**(1): 158-166.
[86] Dehdashti Akhavan N, Umana-Membreno G A, Gu R, *et al*. Optimization of Superlattice Barrier HgCdTe nBn Infrared Photodetectors Based on an NEGF Approach [J]. *IEEE Transactions on Electron Devices*, 2018, **65**(2): 591-598.
[87] Dehzangi A, Haddadi A, Chevallier R, *et al*. Fabrication of 12 μm pixel-pitch 1280 × 1024 extended short wavelength infrared focal plane array using heterojunction type-II superlattice-based photodetectors [J]. *Semiconductor Science and Technology*, 2019, **34**(3): 03LT01.
[88] Gunapala S D, Rafol S B, Ting D Z, *et al*. T2SL meta-surfaced digital focal plane arrays for Earth remote sensing applications [J]. 2019: 9.
[89] Ting D Z, Rafol S B, Keo S A, *et al*. InAs/InAsSb Type-II Superlattice Mid-Wavelength Infrared Focal Plane Array With Significantly Higher Operating Temperature Than InSb [J]. *IEEE Photonics Journal*, 2018, **10**(6): 1-6.
[90] Gershon G, Avnon E, Brumer M, *et al*. 10 μm pitch family of InSb and XBn detectors for MWIR imaging[C]//Infrared Technology and Applications XLIII. International Society for Optics and Photonics, 2017, **10177**: 101771I.
[91] Klipstein P C, Avnon E, Benny Y, *et al*. Type-II superlattice detector for long-wave infrared imaging[C].Infrared Technology and Applications XLI. International Society for Optics and Photonics, 2015, **9451**: 94510K.
[92] Karni Y, Avnon E, Ezra M B, *et al*. Large format 15 μm pitch XBn

detector[C]. Infrared Technology and Applications XL. International Society for Optics and Photonics, 2014, **9070**: 90701F.
[93] Klipstein P C, Gross Y, Aronov D, *et al*. Low SWaP MWIR detector based on XBn focal plane array[C]. Infrared Technology and Applications XXXIX. International Society for Optics and Photonics, 2013, **8704**: 87041S.
[94] Chen Y, Wang Y, Wang Z, *et al*. Unipolar barrier photodetectors based on van der Waals heterostructures [J]. *Nature Electronics*, 2021, **4**(5): 357-363.